ZIBELINE INTERNATIONAL™ PUBLISHING

ISSN: 2637-0778 (Online)
CODEN: ECRNAE

Environmental Contaminants Reviews (ECR)

DOI: http://doi.org/10.26480/ecr.02.2025.77.83

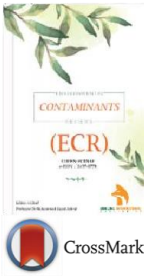

RESEARCH ARTICLE

3D TIME-LAPSE GEOPHYSICAL IMAGING OF FERTILIZER-INDUCED SOIL AND GROUNDWATER CONTAMINATION IN OGHARA, DELTA STATE, NIGERIA

Ozobeme Azubike Anslem[a], Osisanya Olajuwon Wasiu[b*], Airen Osariere John[c], Eyankware O. Moses[d], Iluobe, Oshomah Emmanuel[e]

[a,c] Department of Physics, University of Benin, Benin City, Edo State.
[b] Department of Physics, College of Science, Federal University of Petroleum Resources, Effurun, Delta State.
[d] Department of Geology, Faculty of Science, Dennis Osadebay University, Asaba, Delta State, Nigeria
[e] Department of Applied Geophysics, Federal University of Technology, Akure. Ondo state.
[*]Corresponding Author Email: wasiu.osisanya@uniben.edu

ARTICLE DETAILS

Article History:

Received 19 May 2025
Revised 21 June 2025
Accepted 29 July 2025
Available online 13 August 2025

ABSTRACT

Fertilizer contaminants can persist in subsurface environments, making remediation efforts costly and time-consuming, particularly in areas with shallow aquifers and permeable soils. This study applied time-lapse geophysical methods to assess fertilizer-related soil and groundwater pollution in agricultural regions of Oghara, Delta State, Nigeria. Eight 2-D electrical resistivity imaging (ERI) surveys were conducted, including 16 grid-aligned lines across the Presco lowland and upland areas which were collated to form the 3 D models, along with a control line. Data were processed using RES3DINV and ZondRes3D to produce the 3-D resistivity models. Three-dimensional slices illustrated the downward migration of contaminants over time. Analysis of time-lapse data showed maximum vertical migration rates of 216.7 cm/month and horizontal rates of 750.0 cm/month at the initial site. At the second site, rates reached 122.5 cm/month vertically and 500.0 cm/month horizontally. Taking into account local hydrological and geological conditions, the contaminant plumes are projected to reach the dry sandy layer within 0.5 to 1 year.

KEYWORDS

Resistivity, Depth, slice, Lowland, Fertilizer.

1. INTRODUCTION

Agriculture is acknowledged as a major source of water pollution; however, addressing this issue proves to be particularly difficult due to its geographical context (Eyankware, et al., 2018; Eyankware, et al., 2020). In multiple regions, including Nigeria, many groundwater basins are either currently affected or are at risk of being affected by runoff from irrigated agricultural lands. More than 100 small water systems that have been monitored have reported at least one occurrence of nitrate contamination surpassing the maximum contaminant level (MCL) set for nitrates (Harter et al., 2012). In Nigeria, groundwater is the primary source of drinking water, as well as for industrial and agricultural use. The deterioration of water quality in agricultural regions is primarily attributed to the application of fertilizers and pesticides, which result in the runoff of chemicals and surplus nutrients, such as nitrates, phosphates, and potassium from the fields, ultimately leading to groundwater infiltration (Opoku, et al., 2020; Igwe, et al., 2021). Globally, pesticides and fertilizers serve as essential chemicals employed in various forms such as herbicides, insecticides, fungicides, rodenticides, nematicides, and plant growth regulators. These substances are instrumental in controlling weeds, insects, and diseases affecting crops, while also safeguarding the health of humans and animals (Verma and Kumar, 2023; Odesa, et al., 2024a). The benefits associated with pesticide usage include increased agricultural productivity and a significant reduction in vector-borne diseases. On the contrary, the over application of fertilizers presents a risk to groundwater resources (Wang et al., 2019; Eyankware, et al., 2023a; Odesa, et al., 2024b). Agricultural runoff is defined as surface water that escapes from farmlands when there is more incoming water than the soil can absorb. In light of the challenges arising from a burgeoning global population and the detrimental impacts of climate change, it is imperative to develop innovative and sustainable agricultural management strategies that enhance crop yields without compromising soil health (Eyankware, et al., 2025; Omene, et al., 2015). The application of mineral nitrogen (N) and potassium fertilizers is essential in conventional agriculture for achieving optimal yields and ensuring high-quality crops (Kaufmann et al., 2024). Nonetheless, it is crucial to apply these fertilizers at appropriate times and in suitable quantities to avoid contaminating groundwater and surface water, as well as to reduce atmospheric emissions that could negatively impact the climate (Eyankware, et al., 2016; Butterbach-Bahl et al., 2013; Galloway et al., 2004; Eyankware and Ephraim, 2021; Bouwman et al., 2005; Olatuyi et al., 2012). The nitrogen needs of various crops differ, and the required levels of fertilization are influenced by the nitrogen content present in the soil (Drulis et al., 2022). Fertilizers are integral to contemporary agricultural practices as they provide necessary minerals that foster robust crop development and plentiful yields. Even crop varieties known for high productivity may fall short of their maximum potential without a well-balanced fertilizer application. Fertilizers can typically be divided into two main categories: (i) inorganic or chemical fertilizers, which encompass nitrogenous, phosphatic, potassic, and complex fertilizers, and (ii) organic fertilizers, including farmyard manure, bone meal, compost, green manure, among others. The increasing global population has driven the need for intensified agricultural practices, resulting in a greater reliance on fertilizers that are essential for fulfilling worldwide food requirements. Research conducted during the 1970s and 1980s indicated that one-third of the overall increase in cereal production globally and half of the growth in grain output in India was attributable to the elevated usage of fertilizers (FAO, 2013). In order to sustain a population of 6,127.7 million in the year 2000, the application rates for nitrogen (N), phosphorus (P), and potassium (K)—the primary

Quick Response Code	Access this article online	
	Website: www.contaminantsreviews.com	DOI: 10.26480/ecr.02.2025.77.83

Cite The Article: Ozobeme Azubike Anslem, Osisanya Olajuwon Wasiu, Airen Osariere John, Eyankware O. Moses, Iluobe, Oshomah Emmanuel (2025). 3D Time-Lapse Geophysical Imaging of Fertilizer-Induced Soil and Groundwater Contamination in Oghara, Delta State, Nigeria. *Environmental Contaminants Reviews, 8(2):* 77-83.

constituents of inorganic fertilizers—were recorded at 64.9, 25.9, and 18. By the year 2014, as the worldwide population hit 7,243.8 million, the metrics had escalated to 85.8, 33.2, and 20.4 kilograms per hectare (FAO, 2013). In addition, the total consumption of fertilizer nutrients (N + P_2O_5 + K_2O) was projected at 170.7 million tons for 2010 and 175.7 million tons for 2011. The dependency of global agricultural output on fertilizers is apparent, with forecasts indicating that the consumption of nitrogen (N), phosphorus (P), and potassium (K) fertilizers is anticipated to surge by 172%, 175%, and 150%, respectively, by the year 2050. Moreover, there has been a notable rise in the proportion of urea within global nitrogen production, which currently represents approximately 40% of all nitrogen fertilizers manufactured (Constant and Sheldrick, 1992). The heightened application of fertilizers has resulted in alterations to the nutrient composition of runoff and leachate, causing a deterioration in soil health and adversely affecting the quality of both surface and groundwater. The unregulated and extensive use of fertilizers has emerged as a significant factor in the pollution of soil and water, endangering both untouched terrestrial and aquatic ecosystems downstream, as well as posing threats to human health. While soils inherently contain heavy metals (HMs) such as cadmium (Cd), mercury (Hg), arsenic (As), chromium (Cr), and lead (Pb), the overuse of fertilizers exacerbates the problem by reducing soil pH, which in turn enhances the availability of these metals. Furthermore, fertilizers may also introduce various HMs from their raw materials, thereby increasing the heavy metal concentration within the soil.

Geophysical surveys are becoming increasingly prevalent in agriculture for mapping objectives, as the high-throughput acquisition of geophysical properties, such as electrical conductivity (the reciprocal of resistivity), can indicate key soil features including moisture, texture, and salinity (Eyankware and Aleke, 2021; Akinseye, et al., 2023). By employing non-invasive geophysical techniques, farmers can gain valuable insights into the spatial and temporal distribution of soil nutrients, thereby enhancing their fertilization and crop management practices. Nonetheless, this study primarily emphasizes the effectiveness of time-lapse geophysical surveys in characterizing system dynamics. Analyzing the impacts of agricultural practices over the course of the growing season can provide crucial information that benefits crop production. This study illustrates the use of time-lapse electrical resistivity tomography (ERT) through two case studies that showcase prevalent agricultural practices, including cover cropping, irrigation-induced compaction, and tillage accompanied by nitrogen fertilization. Additionally, it features physicochemical assessments of soil and water samples to evaluate the degree of fertilizer contamination in both the soil and groundwater located beneath the surface. This research aims to assess the extent and behavior of fertilizer-induced soil and groundwater contamination in agricultural areas of Oghara, Delta State, Nigeria, using two-dimensional and three-dimensional electrical resistivity tomography, with the objectives of generating resistivity models to identify and track contaminant plumes and evaluate their spatial and temporal migration.

2. Location, Climate, and Topography

The study was carried out in the mangrove swamp of Delta State, situated between the longitudes of 005° 34' 05.74" E and 005° 34' 12.50" E, as well as the latitudes of 05° 57' 50.87" N and 05° 57' 57.89" N, at PRESCO farmland, where elevations range from 13 to 33 meters. Furthermore, the research encompassed longitudes from 005° 36' 12.80" E to 005° 36' 17.41" E and latitudes from 06° 0' 29.13" N to 06° 0' 36.08" N, with elevations between 6 to 18 meters in Ugbekun farmland. Both farmlands, PRESCO and UGBEKUN, are situated within the Oghara Local Government Area of Delta State. Rainfall is predominantly observed from April to October, with yearly precipitation usually falling between 2000mm and 3000mm, alongside strong sunlight for a minimum of 8 hours daily. Throughout the year, temperatures tend to remain elevated, especially from November to April, with a monthly average close to 31°C. The fluctuation in annual temperature is slight, varying merely between 3°C and 5°C. Relative humidity levels fluctuate from 90% during the rainy months to approximately 60% in the dry months (Iloeji, 2003; Eyankware, et al., 2024). In Delta State, there are three distinct soil types. These consist of alluvial soils found on marine deposits along the coast, alluvial and hydromorphic soils situated on marine and lacustrine deposits adjacent to the Niger and Benin Rivers, and feral soils located on loose sandy sediments in the dry land areas of the north and northeast (Iloeji, 2003; Umeri et al., 2016).

3. Geology and Hydrogeology of The Study Area.

The research area is situated in the Niger Delta Basin, it is an extensional rift basin located in the Niger Delta and the Gulf of Guinea on the passive continental margin near the western coast of Nigeria. The Niger delta basin is one of the largest subaerial basins in Africa. It has a subaerial area of about 75,000 km^2, a total area of 300,000 km^2, and a sediment fill of 500,000 km^3. The sediment fill has a depth between 9 to 12 km. It is composed of several different geologic formations that indicate how this basin could have formed and characterized by the Sombreiro Deltaic Features and the Benin Formation. This region encompasses three primary sedimentary environments: marine, mixed, and continental. According to the classification of sedimentary environments, the sedimentary sequence is delineated by three distinct rock formations: Benin, Agbada, and Akata. In communities within the Niger Delta that engage in oil production, the source and seal rocks comprise the marine/deltaic, plastic, and over-pressured shales found in the Akata and Agbada Formations (Chambers et al., 2006). The geological characteristics of the study area include Clay, Sand, Pebbles, Sandstone, Gravel, Shales, Mangrove Swamp, Lignite, and Alluvium. The aquifers associated with the Benin Formation fulfill the groundwater requirements of the region, where the poorly sorted coastal sands become progressively more sandy and unconsolidated as one approaches the surface. These conditions enhance both porosity and permeability, subsequently elevating the storage coefficient of the aquifer. Recharge from adjacent water bodies, along with significant rainfall and minimal runoff due to the dense vegetation, is limited. Consequently, this has led to the establishment of a highly productive hydrologic unit in the region.

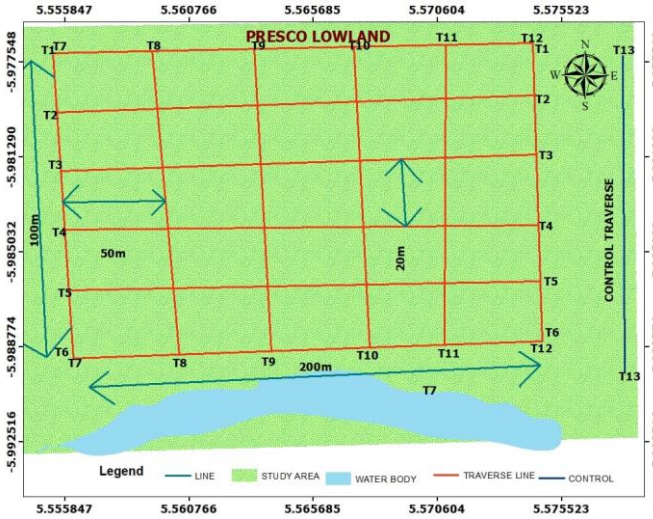

Figure 1: Base Map of the study area

4. Methodology

4.1 Data Acquisition

4.2 2-D and 3-D Electrical Resistivity Imaging

The resistivity data from each survey line were formatted to be compatible with the RES2DINV inversion software. Given that the surveyed terrain was predominantly flat, no elevation corrections were necessary for the recorded measurements. The inversion of the 2D data was carried out using the RES2DINV program. In total, twelve (12) traverses were gathered, comprising (4) 2D traverses from each of the two distinct seasons, as depicted in Figure 1, arranged in a grid format. This dataset includes thirteen (4) traverses from the initial site, twelve (3) from the subsequent site, and one (1) traverse identified as a control profile. The Wenner array electrode was employed to collect the 2D resistivity imaging data. This configuration is particularly suited for systems requiring consistent spacing, facilitating the simultaneous acquisition of multiple data points during each current injection. 2D resistivity survey was executed using the PASI Terrameter, with measurements recorded at electrode intervals of 10 m, 20 m, 30 m, 40 m, 50 m, and 60 m, employing a total of four (4) electrodes for all traverses, each spanning a distance of 200 m.

5. Results and Discussion

5.1 Discussion of ERT Resistivity Method – Presco (Low Land)

5.2 Detailed Investigation: Discussion of The 3-D Results (First and Second Season)

5.2.1. 3-D Horizontal Depth Slice of Low Land and Presco Up Land

5.2.2. 3-D Horizontal Depth Slice Presco Low land (First Season)

The horizontal 3D depth slices derived from the 3-D inverted resistivity structure at Presco low land (refer to Figure 2) penetrated 34.3 m into the subsurface, revealing resistivity values that varied between 352 and 3182

Ωm throughout the depth slice. In the depth range of 0 to 2.5 m, the data indicates the presence of sand contaminated by fertilizer, with resistivity values between 600 and 3182 Ωm. Meanwhile, at a depth of 2.5 to 5.38 m, the analysis identifies a mixture of sand affected by a fertilizer plume and uncontaminated sand, showing resistivity values from 352 to 2323 Ωm. Between depths of 5.38 and 8.68 meters, the sand is found to be contaminated with artificial fertilizer, alongside uncontaminated sand. The interval from 8.68 to 12.5 meters exhibits characteristics indicative of sand that is both contaminated with artificial fertilizer and uncontaminated sand, displaying resistivity values that range from 352 to 1238 Ωm. Furthermore, the subsurface analysis from depths of 12.5 to 16.9 meters reveals that the geoelectric structure indicates the presence of a fertilizer plume contaminating the sand, as well as uncontaminated sand, again with resistivity values between 352 and 1238 Ωm. The resistivity structure exhibits comparable alterations from depths of 16.9 to 34.3 meters in the subsurface, indicative of sand that is affected by a fertilizer plume alongside uncontaminated sand, with resistivity values between 482 and 1238 Ωm. This suggests that the presence of the fertilizer leachate plume is more significant at depths ranging from 0 to 12.5 m.

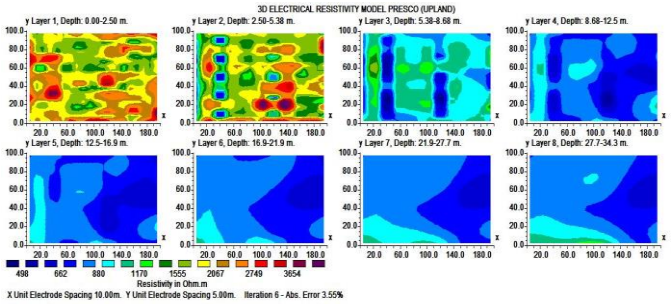

Figure 2: Horizontal Depth Slices obtained from the 3D Inversion Presco Lowland (First Season).

5.2.3. 3-D Horizontal Depth Slice Presco Upland (First Season)

The horizontal 3D depth slices derived from the 3-D inverted resistivity structure at Presco upland (refer to Figure 3) successfully penetrated 34.3 meters below the surface, revealing resistivity values that varied between 498 and 3658 Ωm throughout the depth slice. In the subsurface layer ranging from 0 to 2.5 meters, the data reflects a mixture of sand that is both contaminated by a fertilizer plume and uncontaminated sand, with resistivity values falling between 1170 and 3654 Ωm. Meanwhile, at a depth extending from 2.5 to 5.38 meters, the analysis indicates the presence of sand affected by the fertilizer plume alongside uncontaminated sand, with resistivity values ranging from 498 to 2057 Ωm. Between depths of 5.38 and 8.68 meters, the soil consists of sand that is contaminated with artificial fertilizer as well as uncontaminated sand, exhibiting resistivity values between 498 and 1170 Ωm. In the interval from 8.68 to 34.3 meters, a similar resistivity pattern was observed, indicative of both fertilizer-contaminated and uncontaminated sand, with resistivity values from 498 to 880 Ωm. This data indicates that the leachate plume from the fertilizer is more pronounced within the depth range of 0 to 34.3 meters.

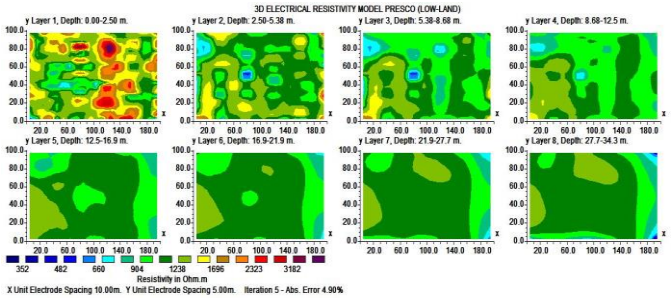

Figure 3: Horizontal Depth Slices obtained from the 3D Inversion Presco Upland (First Season).

5.2.4. 3-D Horizontal Depth Slice Presco Low land (Second Season)

The horizontal 3D depth slices derived from the 3-D inverted resistivity data at Presco low land (as illustrated in Figure 4) successfully penetrated 34.3 meters into the subsurface, revealing resistivity values that varied from 80.9 to 10,427 Ωm throughout the depth slice. In the subsurface depth interval of 0 to 2.5 meters, the results indicate the presence of sand contaminated with fertilizer, exhibiting resistivity values between 80.9 and 2,602 Ωm. Meanwhile, the depth range from 2.5 to 5.38 meters reflects a mixture of sand impacted by a fertilizer plume and uncontaminated sand, with resistivity values spanning from 324 to 2,602 Ωm. Between depths of 5.38 and 8.68 m, there are observed pockets of sand that are tainted with an artificial fertilizer plume, alongside uncontaminated sand displaying resistivity values between 80.9 and 2602 Ωm. In the interval from 8.68 to 16.9 m, a similar pattern of resistivity structures is evident, indicating the presence of both contaminated and uncontaminated sand, with resistivity values that fall within the range of 80.9 to 649 Ωm. Furthermore, the subsurface analysis from 16.9 to 21.9 m reveals a geoelectric structure characterized by sand affected by the fertilizer plume as well as uncontaminated sand, with resistivity values from 324 to 649 Ωm. Between depths of 21.9 and 34.3 meters, the subsurface is characterized by uncontaminated sand, exhibiting resistivity values that vary from 649 to 1299 Ωm. This indicates that the presence of the fertilizer leachate plume is more prominent at depths ranging from 0 to 16.9 meters.

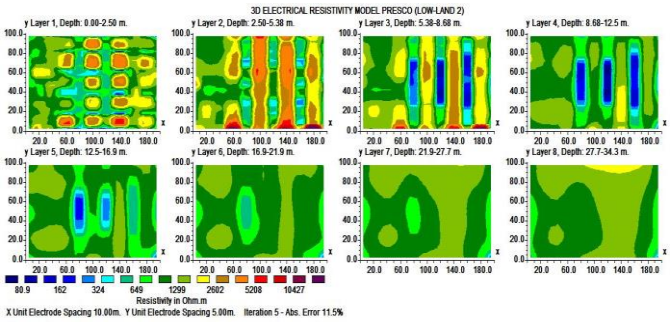

Figure 4: Horizontal Depth Slices obtained from the 3D Inversion Presco Low land (Second Season)

5.2.5. 3-D Horizontal Depth Slice Presco Up land (Second Season)

The horizontal 3D depth slices derived from the 3-D inverted resistivity structure at Presco Up land (refer to Figure 5) successfully penetrated 34.3 m into the subsurface, revealing resistivity values fluctuating between 109 and 2297 Ωm throughout the depth profile. In the depth range of 0 to 2.5 m below the surface, the findings indicate the presence of sand tainted by fertilizer, characterized by elevated resistivity values between 1248 and 2297 Ωm. Between depths of 2.5 and 8.68 m, the analysis shows both high and low concentrations of sand affected by a fertilizer plume, with resistivity values ranging from 678 to 2297 Ωm. Additionally, from 8.68 to 12.5 m deep, the samples consist of sand contaminated with artificial fertilizer alongside uncontaminated sand, exhibiting resistivity values from 678 to 1248 Ωm. The interval from 12.5 to 16.9 m indicates the presence of sand that is affected by artificial fertilizer contamination, alongside uncontaminated sand, exhibiting resistivity values between 678 and 1248 Ωm. Meanwhile, the depth range of 16.9 to 21.9 m reveals a geoelectric structure characterized by sand contaminated by a fertilizer plume and uncontaminated sand, with resistivity values spanning from 368 to 1248 Ωm. Similar alterations in the resistivity structure are observed within the depth range of 21.9 to 34.3 meters in the subsurface, indicating the presence of sand affected by a fertilizer plume and uncontaminated sand, with resistivity values varying from 200 to 1248 Ωm. This suggests that the fertilizer leachate plume is notably more significant between the depths of 0 and 34.3 m.

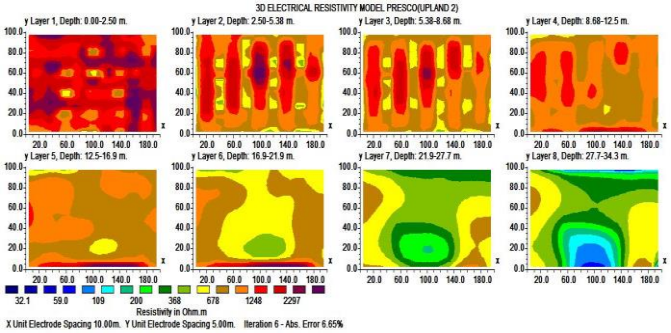

Figure 5: Horizontal Depth Slices obtained from the 3D Inversion Presco Upland (Second Season).

5.3 3-D MODEL OF PRESCO LOWLAN AND PRESCO UPLAND

5.3.1. 3-D Electrical Resistivity Model Presco Low land (First Season).

Figure 6, illustrates the 3-D resistivity model created from the resistivity data collected in the low-land area. Within this model, the resistivity values varied between 100 Ωm and 10,000 Ωm, corresponding to a depth

of 50 m. Nonetheless, the insights gleaned from this 3D block are rather limited. Analysis of the depth slices derived from the model revealed a trend of decreasing resistivity values with increasing depth. Specifically, for the depth range of 0 to 2.5 m, resistivity values spanned from approximately 660 Ωm to 3182 Ωm. Meanwhile, at depths of 2.5 to 5.0 m, the peak resistivity reached about 2323 Ωm, with the minimum being around 482 Ωm. At the maximum probing 8depth of 34.3 m, the highest resistivity value observed was approximately 1238 Ωm. The findings indicated a notable inhomogeneity in the subsurface characteristics of the study area. Additionally, an analysis of the depth slices identified a persistent low resistivity region located at approximately x = 90 m and y = 50 m. This pattern implies the presence of a fertilizer contaminant plume that has migrated from the surface to a depth estimated at around 21.9 m.

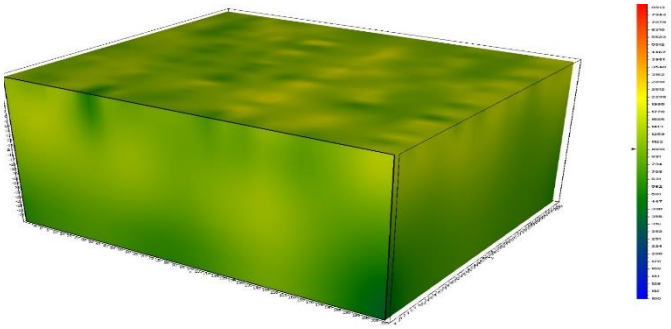

Figure 6: 3D Model Presco Low land (First Season).

5.3.2. 3-D Electrical Resistivity Model Presco Upland (First Season).

Displayed in Figure 7, is the 3-D resistivity model created from resistivity data collected in the up-land region. The resistivity values in this three-dimensional model span from 100 Ωm to 10,000 Ωm over a depth of 50 m. Upon analyzing the 3D model alongside the available depth slices, three distinct resistivity zones were identified. The uppermost zone, which extends from 0.0 to 5.38 meters, is classified as the first resistivity zone, exhibiting values between approximately 662 Ωm and 3,654 Ωm. This particular zone is significantly influenced by human activities, notably the potential contamination from fertilizers characterized by a high resistivity pollutant. The second resistivity zone is identified within the depth range of 5.38 to 8.68 meters, exhibiting resistivity values between 498 Ωm and 1555 Ωm. This zone is regarded as a transitional area, characterized by traces of subsoil exhibiting relatively high resistivity. The third resistivity zone extends from a depth of 8.68 meters to 34.3 m.

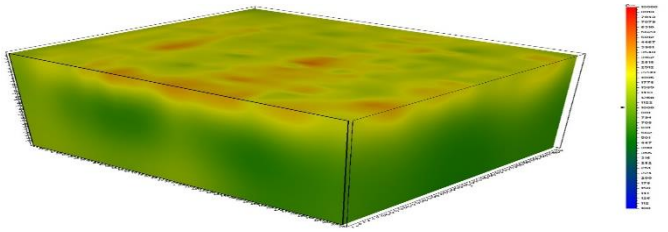

Figure 7: 3D Model Presco Upland (First Season).

5.3.3. 3-D Electrical Resistivity Model Presco Low land (Second Season).

Figure 8, illustrates the 3-D resistivity model derived from subsequent resistivity data collected in the vicinity of the Presco upland region. Within this block, the resistivity values span from 100 Ωm to 10,000 Ωm to a depth of 50 m. An integrated analysis of the 3D model alongside the corresponding depth slices reveals that the resistivity values for the depth range of 0 to 10.0 m fall between 10.9 Ωm and 10,427 Ωm. This particular zone is the most significantly influenced by human activities, resulting in the greatest degree of inhomogeneity. At depths ranging from 10 to 34.3 m, the 3-D model indicates resistivity values between <80.9 Ωm and 1,299 Ωm. This resistivity range is typically indicative of the background resistivity characteristics of the subsurface. Nevertheless, three distinct low resistivity zones were observed within the coordinates of x= 70 - 170 m and y= 10 – 70 m. These zones 2were particularly pronounced starting at a depth of 5.38 m and began to fade away at a depth of 21.9 m. This observation indicates that a low resistivity fluid, presumably a fertilizer contaminant plume, is concentrated within this specific depth interval.

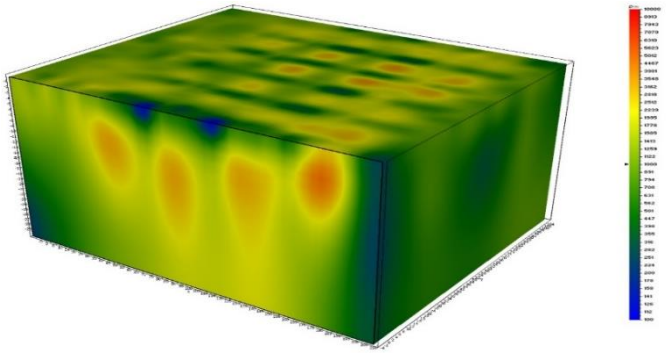

Figure 8: 3D Model Presco Low land (Second Season).

5.3.4. 3-D Electrical Resistivity Model Presco Upland (Second Season).

Displayed in Figure 9, is the 3-D resistivity model created from the follow-up resistivity data collected in the upland region. The resistivity values observed within this three-dimensional model span from 100 Ωm to 10,000 Ωm. An integrated analysis of the 3D block alongside the available depth slices has revealed the presence of three distinct resistivity zones. The uppermost zone, extending from 0.0 to 12.5 meters, constitutes the first resistivity zone, characterized by values that range from approximately 1248 Ωm to over 2297 Ωm. This zone is believed to be significantly influenced by the presence of high resistivity pollutants, as well as other anthropogenic factors affecting this area. The second resistivity zone, characterized by resistivity values ranging from 368 Ωm to 1248 Ωm, spans from a depth of 12.5 m to 21.9 m and is identified as the transition zone. Following this, the third resistivity zone commences at 21.9 m and reaches the maximum probing depth of 34.3 to 50 m. Within this third zone, resistivity values vary between less than 32.1 Ωm and 678 Ωm. This zone is indicative of the background resistivity of the subsurface in the region; however, there are indications of the early presence of the suspected contaminant. It can be inferred that the plume of fertilizer contaminants has penetrated vertically to depths exceeding 50 m in certain locations, and its effects appear to be intensifying. Studies conducted elsewhere showed same result (Eluwole, et al., 2021; Wang, et al., 2015).

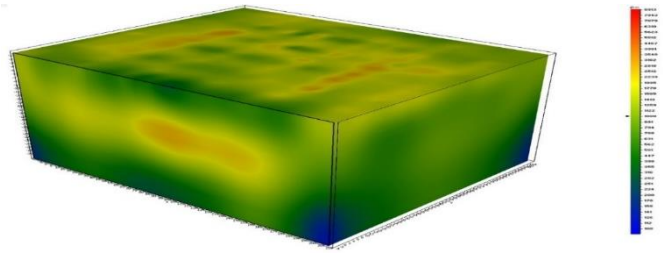

Figure 9: 3D Model Presco Up land (Second Season).

5.4 Fertilizer Contaminants Plume Zones Resistivities in the Survey Period

The identification of fertilizer plumes occurred both at the surface and subsurface levels, exhibiting resistivity values that ranged from 109 Ωm to 2862 Ωm in the presence of sand. Consequently, the representative resistivity values for each plume zone across various survey periods were easily discernible on the color bars of the 2-D resistivity structures. These findings are presented in Tables 1 and 2.

Table 1: Electrical Resistivities of Plume Zones in the Presco Low Land at the different Periods

PLUME TRAVERSE NO.	SURVEYED DATE	RESISTIVITY(Ωm)	REMARKS
ERT1	6/04/2023	781-832	The fertilizer plume observed in 2023 was present in 2024 display. It may have been concentrated with excess fertilizer plume/leachate which is responsible for the decrease in resistivity.
ERT1	11/04/2024	128-355	

Table 1 (cont): Electrical Resistivities of Plume Zones in the Presco Low Land at the different Periods			
ERT3	6/04/2023	800-1041	The plume observed in 2023 was present in 2024 display. It may have been diluted with water for the concentration to be reduced which is responsible for the increase in resistivity
ERT3	11/04/2024	771-944	
ERT6	6/04/2023	731-935	The plume observed in 2023 was present in 2024 display. It may have been diluted with water for the concentration to be reduced which is responsible for the increase in resistivity.
ERT6	11/04/2024	677-954	
ERT7	6/04/2023	531-737	The plume observed in 2023 was present in 2024 display. It may have been diluted with water for the concentration to be reduced which is responsible for the increase in resistivity
ERT7	11/04/2024	109-258	
ERT8	6/04/2023	531-1050	The plume observed in 2023 was present in 2024 display. It may have been diluted with water for the concentration to be reduced which is responsible for the increase in resistivity
ERT8	11/04/2024	261-989	
ERT9	6/04/2023	677-923	The plume observed in 2023 was present in 2024 display. It may have been diluted with water for the concentration to be reduced which is responsible for the increase in resistivity
ERT9	11/04/2024	109-563	
ERT11	6/04/2023	776-2862	The plume observed in 2023 was present in 2024 display. It may have been diluted with water for the concentration to be reduced which is responsible for the increase in resistivity
ERT11	11/04/2024	283-443	
ERT13	6/04/2023	596-887	The plume observed in 2023 was present in 2023 display. It may have been diluted with water for the concentration to be reduced which is responsible for the increase in resistivity
ERT13	11/04/2024	365-1072	

Table 2: Electrical Resistivities of Plume Zones in the Presco Upland at the different Periods			
PLUME TRAVERSE NO.	**SURVEYED DATE**	**RESISTIVITY(Ωm)**	**REMARKS**
ERT17	6/04/2023	592-887	The plume observed in 2023 was present in 2024 display. It may have been diluted with water for the concentration to be reduced which is responsible for the increase in resistivity.
ERT17	11/04/2024	365-1072	
ERT18	6/04/2023	633-929	The plume observed in 2023 was present in 2024 display. It may have been diluted with water for the concentration to be reduced which is responsible for the increase in resistivity.
ERT18	11/04/2024	286-1348	
ERT20	6/04/2023	673-1007	The plume observed in 2023 was present in 2024 display. It may have been diluted with water for the concentration to be reduced which is responsible for the increase in resistivity.
ERT20	11/04/2024	675-925	

5.5 Discussion of Time Lapse Study

Comprehensive analysis of soil and water samples indicated that both sites are impacted by the presence of fertilizer contamination plumes (Samouëlian, et al., 2005). The presence of fertilizer leachate plumes was identified in the first site (Presco lowland), and a subsequent time lapse study was conducted to validate the findings from the 2023 ERT survey. The resistivity measurements obtained during the 2024 survey for certain lines ranged from 109 Ωm to 2862 Ωm, corroborating the interpretations made in 2023. Furthermore, the time lapse study in the Presco lowland aimed at tracking the movement of contaminant plumes revealed that the highest vertical migration rate of contaminants in this location is 216.7 cm/month, while the horizontal migration rate is noted to be 750.0 cm/month, respectively. A time lapse analysis conducted at the second site (Presco upland) to observe the movement of contaminant plumes reveals that the highest rate of vertical contaminant migration in the subsurface at this location is 122.5 cm/month, while the horizontal migration is measured at 500.0 cm/month. These findings indicate that both 2study

locations, the first and the second, remain significantly active at the time of this assessment. This is in line with studies conducted by (Fajana, et al., 2020). Detailed calculations of the migration rates are provided in Table 3 and Table 4.

Table 3: Result of Time lapse study of the Pesco Lowland

PLUME TRAVERSE NO.	Date	Vertical Position (m)	Horizontal Position (m)	Vertical Migration (m)	Horizontal Migration (m)	Vertical Migration Rate (cm/month)	Horizontal Migration Rate (cm/month)
ERT1	6/08/14	2.8	8.0	10.0	22.0	83.3	183.3
	11/08/15	12.8	30.0				
ERT3	6/08/14	12.8	90.0	26.8	10.0	216.7	83.3
	11/08/15	39.6	80.0				
ERT6	6/08/14	39.6	75.0	21.1	15.0	175.8	125.0
	11/08/15	18.5	90.0				
ERT7	6/08/14	24.9	95.0	14.7	50.0	122.5	416.7
	11/08/15	39.6	40.0				
ERT8	6/08/14	18.5	120.0	6.4	80		
	11/08/15	24.9	40.0			53.3	666.7

Table 4: Result of Time lapse study of the Presco Upland

Plume No.	Date	Vertical Position (m)	Horizontal Position (m)	Vertical Migration (m)	Horizontal Migration (m)	Vertical Migration Rate (cm/month)	Horizontal Migration Rate (cm/month)
ERT17	5/08/2014	31.9	80.0	7.7	60.0	64.2	500.0
	10/08/2015	39.6	140.0				
ERT18	5/08/2014	24.9	200.0	14.7	40.0	122.5	333.3
	10/08/2015	39.6	160.0				
ERT21	5/08/2014	24.9	180.0	14.7	20.0	122.5	166.7
	10/08/2015	39.6	200.0				

The inaugural ERT survey, during the dry season, which the fertilizer contaminant plumes were mapped out. A subsequent ERT survey was carried out precisely one year later, in April 2024, at which point the fertilizer contaminant plumes likely experienced dilution due to additional infiltrating water or the introduction of further fertilizer leachate, resulting in an accelerated movement both vertically and horizontally.

The velocity of migration is influenced by the soil's porosity and permeability, as well as the topographical features of the area. Notably, migration rates differ between the first and second locations. Nonetheless, it is indicated that if the vertical migration rate remains consistent within the dry sand layer—averaging approximately 13.7 meters in thickness based on borehole drilling data—it would take around 0.5 years for the fertilizer contaminant plume in the first location and about 1 year for that in the second location to reach the saturated sandy layer situated directly beneath.

Furthermore, it has been observed that the horizontal migration rate surpasses the vertical migration rate, with differences of 133.4 cm/month and 210.8 cm/month in the second and third cemeteries, respectively.

Table 5: Migrating plume arrival time in subsoil in the different locations

Location	Maximum vertical migration rate(m/month)	Surface layer average thickness(m)	Predicted arrival time in the underlying sandy soil (years)
First location (Presco Lowland)	2.167	13.7	0.5
Second Location (Presco Upland)	1.225	13.7	1

6. Conclusion

This study presents the subsequent findings:

- The three-dimensional depth slices generated from the electrical resistivity model have disclosed the distribution of fertilizer contaminants within the resistivity structures of the study areas. These 3-D slices indicate that the fertilizer contamination is progressively migrating downward as depth increases.
- The three-dimensional (3-D) electrical resistivity model has illustrated the volumetric distribution of resistivity within the study areas. Notably, there is evidence of fertilizer contamination present both at the surface and subsurface levels in the southeastern region of the study area.
- Between 2023 and 2024, a variation in the resistivity of the fertilizer leachate plume has been observed in the areas under examination, attributed to the temporal migration of the fertilizer contaminant plume.
- When comparing the migration of fertilizer contaminant plumes at the first location to those at the second location, it is evident that the former extends laterally and penetrates deeper, with only a few instances occurring near the surface.
- In a dry sandy area, assuming a consistent vertical migration rate, the fertilizer leachate plume originating from the study site is projected to reach the subsequent subsurface zone within an average timeframe of 0.5 to 1 year.

Recommendations

- Collaboration among farmers, industrial sectors, and regulatory bodies is essential for the effective enforcement of environmental regulations and guidelines. This partnership should also prioritize the implementation of pump and treat systems (PTS) to extract contaminated groundwater, which must subsequently undergo treatment through filtration or chemical processes.
- Furthermore, the practice of bioremediation should be adopted by introducing specific microorganisms capable of naturally breaking down pollutants. Additionally, phytoremediation techniques should be employed, utilizing plants that can absorb and mitigate contaminants present in both soil and water.

References

Akinseye, V.O., · Osisanya, W.O., M. O. Eyankware., Korode, I.A.., Ibitoye, A.T., 2023. Application of second-order geoelectric indices in determination of groundwater vulnerability in hard rock terrain in

SW. Nigeria. Sustainable Water Resources Management. 9:169, https://doi.org/10.1007/s40899-023-00936-w

Bouwman, A. F., Van Drecht , G., Knoop , J. M., Beusen , A. H. W. and Meinardi, C.R., 2005. Exploring changes in river nitrogen export to the world's oceans. Global Biogeochem. Cycles 19:GB1002. doi:10.1029/2004GB002314.

Butterbach-Bahl, K., Baggs, E.M., Dannenmann, M., Kiese, R. and Zechmeister-Boltenstern, S., 2013. Nitrous oxide emissions from soils: how well do we understand the processes and their controls.Philosophical Transactions of the Royal Society B: Biological Science, 368 doi: 10.1098/rstb.2013.0122. 20130122–20130122.

Chambers, J.E., Kuras, O., Meldrum, P.I., Ogilvy, R.D., Hollands, J., 2006. Electrical resistivity tomography applied to geologic, hydrogeologic, and engineering investigations at a former waste disposal site. Geophysics 71 (6), Pp. 231-239.https://doi.org/10.1190/1.2360184

Constant KM and Sheldrick WF., 1992. World nitrogen survey. World Bank technical paper number 174. Washington, DC.

Drulis P, Kriaučiūnienė Z, Liakas V., 2022. The Influence of Different Nitrogen Fertilizer Rates, Urease Inhibitors and Biological Preparations on Maize Grain Yield and Yield Structure Elements. Agronomy. 2022; 12(3): Pp. 741. https://doi.org/10.3390/agronomy12030741

Eluwole, A.B., Fajana, A.O., Adeyemi, A.M., Olasupo, T.E., Adebiyi, L.S., Nalla, P.A., 2021. A model tank investigation of the electrical resistivity response over a simulated forensic target. Journal of Applied Geophysics, 194(10), 104440.

Eyankware MO, Aleke G., 2021. Geoelectric investigation to deter mine fracture zones and aquifer vulnerability in southern Benue Trough southeastern Nigeria. Arab J Geosci. https:// doi. org/ 10. 1007/s12517-021-08542-w

Eyankware, M. O. Akakuru, O. C. Igwe, E. O,. Olajuwon, W. O K. P. Ukor., 2024. Pollution Indices, Potential Ecological Risks and Spatial distribution of Heavy Metals in soils around Delta State, Nigeria. Water, air, and soil Pollution. https://doi.org/10.1007/s11270-024-07209-yI

Eyankware, M. O., Aleke, C. G., Selemo, A. O. I., and Nnabo, P. N., 2020. Hydrogeochemical studies and suitability assessment of groundwater quality for irrigation at Warri and environs, Niger delta basin, Nigeria. Groundwater for Sustainable Development. https://doi.org/10.1016/j.gsd.2019.100

Eyankware, M. O., Ephraim, B. E., 2021. A comprehensive review of water quality monitoring and assessment in Delta State Southern part of Nigeria. Journal of Environment and Earth Science. https://doi.org/10.30564/jees.v3i1.2900

Eyankware, M. O., Nnajieze, V. S., and Aleke, C. G., 2018. Geochemical assessment of water quality for irrigation purpose, in abandoned limestone quarry pit at Nkalagu area, Southern Benue Trough Nigeria. Environmental Earth Sciences. https://doi.org/ 10.1007/s12665-018-7232-x

Eyankware, M. O., Obasi, P. N., Akakuru, O. C., 2016. Use of hydrochemical approach in evaluation of water quality around the vicinity of Mkpuma Ekwaoku Mining District, Ebonyi State, SE. Nigeria for irrigation purpose. Indian J Sci 23(88): Pp. 881–895

Eyankware. M. O., Ogwah, C., Umayah, O. S., 2021. Integrated geophysical and hydrogeochemical characterization and assessment of groundwater studies in Adum West Area of Benue State, Nigeria. Journal of Geological Research 65, 65881289. DOI: https://doi.org/10.30564/jgr.v3i3.3197

Fajana, A.O., Ofobutu, H.O.,Eluwole, A.B., 2020. Laboratory modeling for contaminant migration monitoring using electrical resistivity method. Modeling Earth Systems and Environment, 6(2), Pp. 1027-1043.

FAO, 2013. Guidelines to control water pollution from agriculture in China, Water Report 40.

Galloway, J. N., Dentener, F. J., Capone, D. G., Boyer, E. W., Howarth, R. W., Seitzinger, S. P. and Vorosmarty, C. J., 2004. Nitrogen Cycles: Past, Present, and Future. Biogeochemistry, 70(2), Pp. 153–226. doi:10.1007/s10533-004-0370-0

Harter, T., Lund, J., Darby, J., Fogg, G. E., Howitt, R., Jessoe, K. K., Pettygrove, G. S. and Quinn, J. F., 2012. Addressing nitrate in California's drinking water. With a Focus on Tulare Lake Basin andSalinas Valley Groundwater. Report forthe State Water Resources ControlBoard Report to the Legislature. Davis,CA: UC Davis Center for Watershed Sciences.

Igwe, E. O., Ede, C. O., M. O. Eyankware., 2021. Heavy metals concentration and distribution in soils around Oshiri and Ishiagu lead – zinc mining areas, southeastern Nigeria. World Scientific News. 158: Pp. 22-58.

Iloje, S.I., 2003. A General Geography of Nigeria. Heinemann Books Ibadan

Kaufmann, M. S., Klotzsche, A., van der Kruk, J., Langen, A., Vereecken, H., and Weihermüller, L., 2024. Assessing soil fertilization effects using time-lapse electromagnetic induction, EGUsphere, https://doi.org/10.5194/egusphere-2024-2889.

Odesa, G. E. Ozulu, G. U., M. O. Eyankware., Mba-Otike, M. N., Okudibie, E. J., 2024b. A holistic review three-decade oil spillage across the Niger Delta Region, with emphasis on its impact on soil and water. World News of Science. 190(2): Pp. 119-139.

Odesa, G. E., Elozona, O. E., Eyankware,M. O., 2024a. A Review Study on Ecological Equity and Modern Remediation Techniques in Management of Soil. Journal of Pure and Applied Sciences.24.

Olatuyi, S.O., Akinremi, O.O. and Hao, X., 2012. Solute transport in a hummocky landscape: II. Vertical and seasonal redistribution of bromide and ^{15}N-labelled nitrate. Canadian Journal of Soil Science, 92: Pp. 631–643.

Omene, M. E., Chokor, J. U., M. O. Eyankware., 2015.The effects of land use on soil physiochemical properties in Ughelli and its environs, Nigeria. International Journal of Research and Review, India. Vol. 2(11): Pp. 656-67

Opoku-Kwanowaa, Y., Furaha, R. K., Yan, L. and Wei, D., 2020. Effects of planting field on groundwater and surface water pollution in China. CLEAN–Soil, Air, Water, 48(5-6), 1900452

Samouëlian, A., Cousin, I., Tabbagh, A., Bruand, A., and Richard, G., 2005. Electrical resistivity survey in soil science: a review. Soil and Tillage Research, 83(2), Pp. 173-193

Umeri, C. Moseri, H. and Onyemekonwu, R.C., 2016. Effects of nitrogen and phosphorus on the growth performance of maize (Zea mays) in selected soils of Delta State, Nigeria. Advances in Crop Science and Technology, 4 (1): Pp. 1-4

Verma, R. and Kumar, S., 2023. Research onthe Impact of River Pollution on WaterQuality. Social Science Journal forAdvanced Research, 3(4), Pp. 6-11.

Wang, T.P., Chen, C.C., Tong, L.T., Chang, P.Y., Chen, Y.C., Dong, T.H., Cheng, S.N., 2015. Applying FDEM, ERT,and GPR at a site with soil contamination: A case study.Journal of Applied Geophysics,121, Pp. 21-30.